Electronic supplementary materials

For https://doi.org/10.1631/jzus.A2200447

Square cavity flow driven by two mutually facing sliding walls

Bo AN[1,2,3], Josep M. BERGADÀ[4], Weimin SANG[1], Dong LI[1], F. MELLIBOVSKY[5]

[1]*School of Aeronautics, Northwestern Polytechnical University, Xi'an 710072, China*

[2]*National Key Laboratory of Science and Technology on Aerodynamic Design and Research, Xi'an 710072, China*

[3]*Key Laboratory of Icing and Anti/De-icing, China Aerodynamics Research and Development Center, Mianyang 621000, China*

[4]*Department of Fluid Mechanics, Universitat Politécnica de Catalunya, Barcelona 08034, Spain*

[5]*Department of Physics, Aerospace Engineering Division, Universitat Politécnica de Catalunya, Barcelona 08034, Spain*

S1. Validation

Since the present work is an extension from our previous studies [1-2], we will directly use previous data for the validation purpose in the supplementary material.

[1] B. AN, J.M. Bergada, and F. Mellibovsky, "The lid-driven right-angled isosceles triangular cavity flow," Journal of Fluid Mechanics. 875, 476-519. (2019).

[2] B. AN, F. Mellibovsky, J.M. Bergada, and W.M. Sang, "Towards a better understanding of wall-driven square cavity flows using the Lattice Boltzmann method," Applied Mathematical Modelling. 875, 476-519. (2020).

S1.1 Validation for the lid-driven cavity:

Table S1 Comparison of computational results between the results based on the present study and other results at steady Reynolds numbers 1000 and 5000

Re	Positions	Ghia [31]	Rohde [32]	Shi [33]	Hou [34]	Erturk [35]	Present study
1000	Down-left Secondary vortex	X=0.0859	X=0.0807	X=0.0830	X=0.0902	X=0.0833	X=0.0831
		Y=0.0781	Y=0.0759	Y=0.0775	Y=0.0784	Y=0.0783	Y=0.0778
		$\psi = 2.3113\times10^{-4}$	--	--	$\psi = 2.22\times10^{-4}$	$\psi = 2.335\times10^{-4}$	$\psi = 2.284\times10^{-4}$
		$\omega = 0.36175$	--	--	--	$\omega = 0.35427$	$\omega = 0.3462$
	Down-right Secondary vortex	X=0.8594	X=0.8665	X=0.8650	X=0.8667	X=0.8642	X=0.8642
		Y=0.1094	Y=0.1122	Y=0.1130	Y=0.1137	Y=0.1120	Y=0.1120
		$\psi = 1.751\times10^{-3}$	--	--	$\psi = 1.69\times10^{-4}$	$\psi = 1.73\times10^{-4}$	$\psi = 1.732\times10^{-4}$
		$\omega = 1.15465$	--	--	--	$\omega = 1.11822$	$\omega = 1.0921$
	Primary vortex	X=0.5313	X=0.5321	X=0.5315	X=0.5333	X=0.5300	X=0.5311
		Y=0.5625	Y=0.5676	Y=0.5660	Y=0.5647	Y=0.5650	Y=0.5666
		$\psi = -0.11793$	--	--	$\psi = -0.1178$	$\psi = -0.11894$	$\psi = -0.11843$
		$\omega = -2.04968$	--	--	$\omega = -2.076$	$\omega = -2.0677$	$\omega = -2.0672$
Re	Positions	Ghia [31]	Vanka [36]	Das [37]	Hou [34]	Erturk [35]	Present study
	Down-left	X=0.0703	X=0.0625	X=0.0736	X=0.0784	X=0.0733	X=0.0732

	Secondary vortex	Y=0.1367	Y=0.1563	Y=0.1386	Y=0.1373	Y=0.1367	Y=0.1365
		$\psi = 1.3612\times10^{-3}$	--	$\psi = 1.373\times10^{-3}$	$\psi = 1.35\times10^{-3}$	$\psi = 1.3758\times10^{-3}$	$\psi = 1.383\times10^{-3}$
		$\omega = -1.5306$	--	--	--	$\omega = -1.5143$	$\omega = -1.521$
5000	Down-righ t	X=0.8086	X=0.8500	X=0.8017	X=0.8078	X=0.8050	X=0.8051
		Y=0.0742	Y=0.0813	Y=0.0722	Y=0.0745	Y=0.0733	Y=0.0731
	Secondary vortex	$\psi = 3.0836\times10^{-3}$	--	$\psi = 3.123\times10^{-3}$	$\psi = 3.03\times10^{-3}$	$\psi = 3.073\times10^{-3}$	$\psi = 3.089\times10^{-3}$
		$\omega = -2.66354$	--	--	--	$\omega = -2.739$	$\omega = -2.743$
	Primary vortex	X=0.5117	X=0.5125	X=0.5154	X=0.5156	X=0.5150	X=0.5153
		Y=0.5352	Y=0.5313	Y=0.5399	Y=0.5373	Y=0.5350	Y=0.5352
		$\psi = -0.11897$	--	$\psi = -0.1212$	$\psi = -0.1214$	$\psi = -0.12222$	$\psi = -0.1198$
		$\omega = 1.86016$	--	--	--	$\omega = 1.9405$	$\omega = 1.924$

Table S1 introduces the positions of vortices centre and the corresponding values of stream function ψ and vorticity ω on the vortex centres, at steady Reynolds numbers 1000 and 5000.

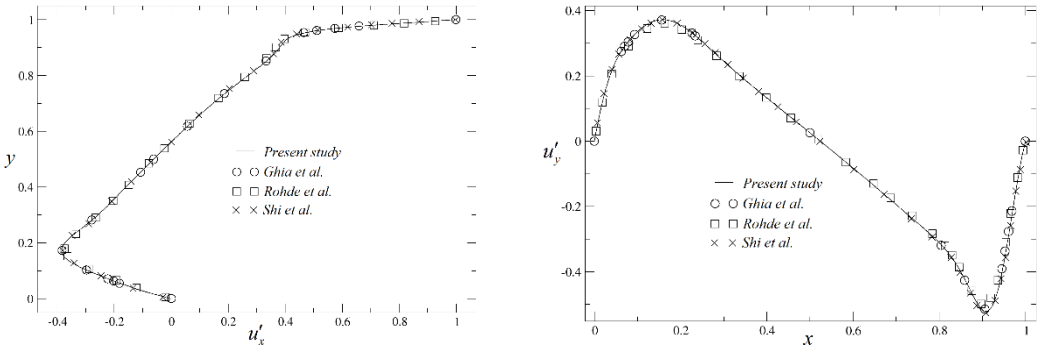

(*a*) (*b*)

Fig. S1 Normalized velocity profiles: (*a*) Horizontal velocity component along the vertical axis. (*b*) Vertical velocity component along the horizontal axis. (*Re* = 1000)

Figure S1 introduces the comparison of the normalized velocity profiles u'_x and u'_y among the present study and the corresponding data presented from references [31-37], where $u'_x = u_x / U_{lid}$ and $u'_y = u_y / U_{lid}$ are defined as the normalized velocity profiles. It is observed that present methodology has a good performance on predicting the steady state at Reynolds number 1000.

At a steady Reynolds number 1000, Table S2 provides a further quantification of the accuracy by measuring the relative error of u_x at the cavity central point with respect to the highest resolution used. It is realised that the relative error is very small whenever resolutions are higher than 200×200. The relative error was calculated when comparing any resolution results to the ones obtained with a resolution of 512×512. Based on this study, it is observed that using resolutions higher than 300×300 at Reynolds 1000 produce very accurate results. Table S3 shows the critical Reynolds number Hopf bifurcation obtained by using present method and other studies.

Table S2. Relative error of different grid spacing over the minimum grid spacing (512×512) at Reynolds number 1000

Resolution	50,50	100,100	200,200	300,300	400,400	512,512

Relative error	0.3912	0.224	0.007687	0.003638	0.001324	0.0

Table S3. Critical Reynolds number of Hopf bifurcation

Resolution	Present LBM	Ref [30-35]	Ref [42]	Ref [43]	Ref [44]	Ref [45]
Re^{H}	8025 ± 25	8000	8018.2 ± 0.6	8026.7	8025.9	8051

[31] U. Ghia, K.N. Ghia, C.T. Shin, "High-Re solutions for incompressible flow using the Navier-Stokes equations and a multigrid method," Journal of Computational Physics, 48, 3, 387-411. (1982)

[32] M. Rohde, D. Kandhai, J.J. Derksen, and E.A. van den Akker, "A generic, mass conservative local grid refinement technique for lattice Boltzmann schemes," International journal for numerical methods in fluids, 51, 439-468. (2006)

[33] X. Shi, X. Huang, Y. Zheng, and T. Ji, "A hybrid algorithm of lattice Boltzmann method and finite difference-based lattice Boltzmann method for viscous flows," International Journal for Numerical Method, 230, 6, 2246-2269. (2011)

[34] S. Hou, Q. Zou, S. Chen, G. Doolen, and A.C. Cogley, "Simulation of cavity flow by the lattice Boltzmann method," Journal of Computational Physics, 118, 2, 329-347. (1995)

[35] E. Erturk, and C. Gökçöl, "Fourth-order compact formulation of Navier-Stokes equations and driven cavity flow at high Reynolds numbers," International Journal for Numerical Methods in Fluids, 50, 4, 421-436. (2005

[36] S. Vanka, "Block implicit multigrid solution of Navier-Stokes equations in primitive variables," Journal of Computational Physics, 65, 1, 138-158. (1986)

[37] M.K. Das, and P. Rajesh Kanna, "Application of an ADI scheme for steady and periodic solutions in a lid-driven cavity problem," International Journal of Numerical Methods for Heat & Fluid Flow, 17, 8, 799-822. (2007)

[42] F. Auteri, N. Parolini, and L. Quartapelle, "Numerical investigation on the stability of singular driven cavity flow," Journal of Computational Physics. 183, 1-25. (2002)

[43] V.B.L. Boppana, and J.S.B. Gajjar, "Global flow instability in a lid-driven cavity," International Journal for Numerical Methods in Fluids. 62, 827-853. (2010)

[44] J.C. Kalita, and B.B. Gogoi, "A biharmonic approach for the global stability analysis of 2D incompressible viscous flows," Applied Mathematical Modelling. 40, 6831-6849. (2016)

[45] A.N. Nuriev, A.G. Egorov and O.N. Zaitseva, "Bifurcation analysis of steady-state flows in the lid-driven cavity," Fluid Dynamics Research. 48, 061405. (2016)

S1.2 Validation for two-sided wall-driven cavity (same code):

In order to further check the performance of the LBM approach used, the velocity profiles along the vertical central line, at $x = 0.5$, and the horizontal central line, at $y = 0.75$, are presented in figure 1. The comparison between the numerical predictions calculated in the present paper and the data from reference [21] is also made to validate the feasibility of LBM model at Reynolds number 1000. It can be seen that the agreement is very good.

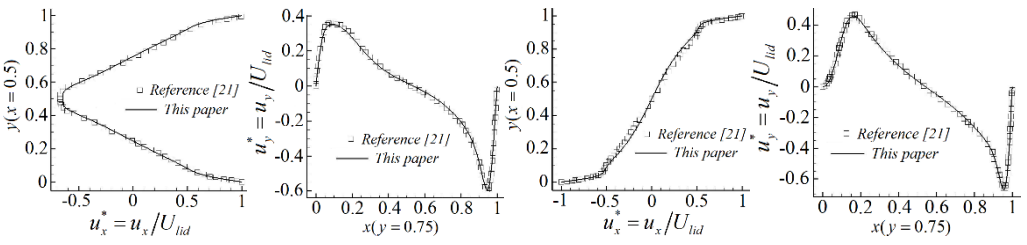

(a) Parallel wall motion (b) Anti-parallel wall motion

Fig. S2. Comparison of the velocity profiles between the computed results from the present paper, cases *S2p* and *S2a*, and the data from reference [21], *Re* =1000

Figure S2 shows several computational results, see Fig. S2, when using different grid resolutions. It is observed that, for the Reynolds number evaluated, *Re*=1000, the grid resolution between 200×200 and 300×300 produces very accurate results. Notice that, in each figure right hand side, the zoomed view of the curve main discrepancy area is presented.

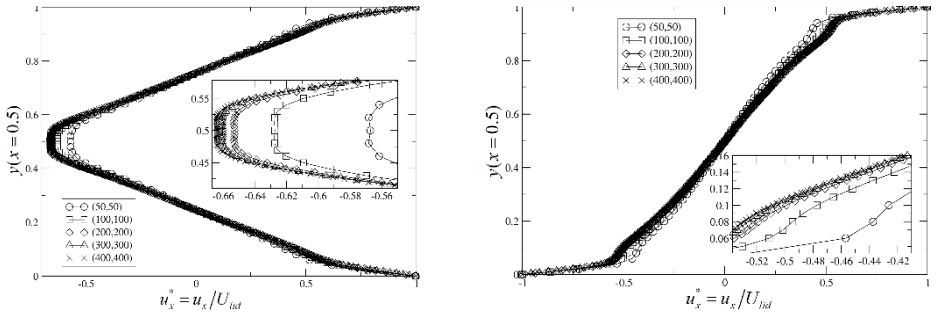

(a) Parallel wall motion (b) Anti-parallel wall motion

Fig. S3. Grid independency test of two-wall driven cavity at *Re* =1000. Each figure shows the zoomed zone where the small disagreement is spotted

Table S4 Frequencies of time series of u_x with different resolutions for parallel wall motion at Reynolds number 9900

Resolution	100,100	200,200	300,300	512,512	800,800	1024,1024
Frequency	steady	steady	steady	1.415658	1.423	1.44095

Table S4 shows the frequencies of a periodic solution based on different resolutions, ranging from 100 to 1024. It is observed that as the Reynolds number increases, the mesh needs to be refined to obtain trustable results.

[21] S. Arun, and A. Satheesh, “Analysis of flow behavior in a two sided lid driven cavity using lattice Boltzmann technique,” Alexandaria Engineering Journal. 54, 4, 795-806. (2015)

S1.3 Validation for lid-driven right-angled isosceles triangular cavity (same code):

Ref/Meth/Res	Prop.	Primary	Bottom left	Bottom right
Ghia *et al.* (1982)	ψ_{vc}	−0.117929	2.31129×10^{-4}	1.75102×10^{-3}
2nd-order FD	ω_{vc}	−2.04968	0.36175	1.15465
257^2	x_{vc}	0.5313	0.0859	0.8594
	y_{vc}	0.5625	0.0781	0.1094
Botella & Peyret (1998)	ψ_{vc}	−0.1189366	2.334528×10^{-4}	1.729717×10^{-3}
Spectral	ω_{vc}	−2.067753	0.3522861	1.109789
160^2	x_{vc}	0.5308	0.0833	0.8640
	y_{vc}	0.5652	0.0781	0.1118
Marchi *et al.* (2009)	ψ_{vc}	−0.118936708	—	—
2nd-order FVM	ω_{vc}	—	—	—
1024^2	x_{vc}	0.53125	—	—
	y_{vc}	0.5652	—	—
Erturk & Gokcol (2006)	ψ_{vc}	−0.118938	2.3345×10^{-4}	1.7297×10^{-3}
4th-order FD	ω_{vc}	−2.067760	0.354271	1.118222
601^2	x_{vc}	0.5300	0.0833	0.8633
	y_{vc}	0.5650	0.0783	0.1117
Bruneau & Saad (2006)	ψ_{vc}	−0.11892	—	1.7292×10^{-3}
2nd-order FD	ω_{vc}	−2.0674	—	1.1120
1024^2	x_{vc}	0.53125	—	0.86426
	y_{vc}	0.56543	—	0.11230
Hou *et al.* (1995)	ψ_{vc}	−0.1178	2.22×10^{-4}	1.69×10^{-3}
LBM	ω_{vc}	−2.076		
513^2	x_{vc}	0.5333	0.0902	0.8667
	y_{vc}	0.5647	0.0784	0.1137
Present work	ψ_{vc}	−0.11664	2.2333×10^{-4}	1.6520×10^{-3}
LBM	ω_{vc}	−2.02059	0.32902	1.0572
301^2	x_{vc}	0.53180	0.08199	0.86436
	y_{vc}	0.56567	0.07815	0.11236
Present work	ψ_{vc}	−0.11773	2.2882×10^{-4}	1.6882×10^{-3}
LBM	ω_{vc}	−2.04311	0.33988	1.0813
601^2	x_{vc}	0.53141	0.08262	0.86427
	y_{vc}	0.56539	0.07815	0.11211
Present work	ψ_{vc}	−0.11815	2.3065×10^{-4}	1.7021×10^{-3}
LBM	ω_{vc}	−2.05210	0.34368	1.0902
1001^2	x_{vc}	0.53125	0.08284	0.86419
	y_{vc}	0.56534	0.07814	0.11204

Fig. S4 Comparison between the result obtained by using present methodology and other peoples' work. Lid-driven right-angled isosceles triangular cavity

S2 Nomenclature

Nomenclature (all parameters are non-dimensional)

c	Lattice speed of LBM
f	Frequency
L	Square cavity side (characteristic length)
L_x	Square size in x direction
L_y	Square size in y direction
M	Mach number
M_x	Mirror symmetry with respect to the horizontal mid-plane
M_y	Mirror symmetry with respect to the vertical mid-plane
N_x	Mesh size in x direction

N_y	Mesh size in y direction
p	Pressure
$\boldsymbol{r}$	Position vector
Re	Bulk Reynolds number
Re_{T}	Top wall Reynolds number
Re_{B}	Bottom wall Reynolds number
T	Period of periodic solutions
t	Time
t_c	Advective time scale
$\boldsymbol{u}$	Velocity vector
$\lvert\hat{u}_x\rvert$	Spectral power density
U	Bulk velocity
U_{T}	Velocity of the top wall
U_{B}	Velocity of the bottom wall
u_x	Horizontal component of velocity
u_y	Vertical component of velocity
α	Top-bottom driving-velocities asymmetry parameter
ρ	Fluid density
ν	Fluid kinematic viscosity
Δx	Grid spacing
Δt	Time step
τ	Relaxation term
$\mathfrak{R}_\pi$	π-rotational symmetry

S3. Equation (S1)

The two-opposing-walls driven square cavity flow problem is invariant under the following symmetry operations

$$\begin{aligned} M_y[u,v,p](x,y,t\,;Re_{\mathrm{T}},Re_{\mathrm{B}}) &= [-u,v,p](-x,y,t\,;-Re_{\mathrm{T}},-Re_{\mathrm{B}}),\\ M_x[u,v,p](x,y,t\,;Re_{\mathrm{T}},Re_{\mathrm{B}}) &= [u,-v,p](x,-y,t\,;Re_{\mathrm{B}},Re_{\mathrm{T}}),\\ \mathfrak{R}_\pi[u,v,p](x,y,t\,;Re_{\mathrm{T}},Re_{\mathrm{B}}) &= [-u,-v,p](-x,-y,t\,;-Re_{\mathrm{B}},-Re_{\mathrm{T}}). \end{aligned} \tag{S1}$$

As a matter of fact, the composition of any two of the symmetries yields the third symmetry. Notice that M_y leaves the problem invariant under the change of sign of both top and bottom velocities, followed by a mirror reflection about the vertical mid-plane ($x = 0$). Meanwhile, M_x consists in the exchange of top and bottom lid velocities followed by a mirror reflection about the horizontal mid-plane ($y = 0$). Finally, both exchanging and inverting the sign of top and bottom lid velocities requires a π-rotation of the flow field to preserve invariance, as specified by symmetry parameter $\mathfrak{R}_\pi$.